

光学学报

基于高阶 LP₂₁模式的鳍豚形可发射光纤传送带

高丙坤, 荣玉菲, 姜春雷*, 陈朋, 水华胜, 吴昊, 董太极, 孙雨, 闫文迪

东北石油大学电气信息工程学院, 黑龙江 大庆 163318

摘要 微粒运输和定向操纵在生物领域和医学新技术方面有着广阔的应用前景。设计了一种鳍豚形光纤光镊结构, 其结合高阶 LP₂₁模式实现了光纤传送带功能。通过将 650 nm 光源输入 155 nm 单模光纤中激发高能量比的 LP₂₁模式, 增强了光纤侧边缘的光场强度。在较低光功率的情况下, 将聚苯乙烯微粒(5 μm)捕获在光纤周围侧边缘处, 并且沿光纤边缘将其运输至尖端处, 最终以粒子枪形式将微粒弹射出去。应用有限元法仿真了鳍豚形光纤探针的光场强度分布, 分析了微粒在光纤上的受力情况, 并在不同光功率下与普通锥形光纤进行了对比实验, 验证了该结构的优越性。该方法设备简单, 为光纤操纵提供了新的可能。

关键词 光纤光学; 微粒运输; 定向操纵; 鳍豚形光纤; LP₂₁模式

中图分类号 Q631 文献标志码 A

DOI: 10.3788/AOS221756

1 引言

非接触式和非破坏性光学操纵, 又称光镊技术, 利用聚焦激光束来捕获、操纵和运输排列微粒或生物细胞。光镊技术最早于 1986 年由 Ashkin 等^[1]提出, 并于 20 世纪 80 年代末应用于生物科学领域。此后, 光镊开始应用于原子物理^[2]、微机械加工^[3]、化学^[4]、生物医学^[5]和微机电系统^[6]等研究领域。同时, 光镊技术在应用发展的基础上也衍生出飞秒^[7]和真空^[8]等其他类别的新型光镊系统, 近年来更是与生物医学新技术广泛结合, 用于细胞的病理性检测^[9]、单个细胞微手术^[10]以及利用病毒、细胞和组织等生物实体设计生物激光器、基于细胞的生物光子波导和生物微透镜^[11]等。在传统光镊基础上发展起来的光纤光镊, 其光路稳定、系统简单、操纵灵活、成本较低, 同时其采用光纤作为光镊的探针, 大大提高了使用的灵活性。正是由于这些优点, 光纤光镊相对于传统光镊具有更广泛的应用前景^[12]。在光纤末端微加工技术发展的基础上, 利用将光纤尖端成形为特殊的锥形形状产生的三维光学力捕获生物粒子, 标志着单光纤光镊的出现^[13]。

随着单光纤光镊技术的发展, 实现各种功能的单光纤光镊层出不穷。最常见的光纤光镊有锥形光纤光镊和微纳光纤光镊。通过机械研磨、熔融拉锥、化学腐蚀甚至 3D 打印^[14]等方法可以将光纤端制备成锥形光纤或者微纳光纤。与此同时, 微粒的运输在细胞生物学应用中体现出较大优势, 从复杂结构的自底向上组

装到生物分析和药物的输送^[15-17]。目前已经提出多种使用外部控制刺激进行粒子和细胞运输的方法, 而光学操纵因其非接触和非破坏的操纵方式迅速发展为运输的有效手段^[18]。许多近场光阱技术, 如等离子体激元^[19-20]、狭缝波导^[21]、纳米光纤^[22-23]和光学微腔^[24], 已被开发用于动态传输和控制微粒的释放^[25-26]。2005 年, Čižmár 等^[27]展示一种可以捕获几个亚微米粒子并在数百微米的距离上进行精确输送的光学传送带, 其需要使用两个反向传播的贝塞尔光束来创建驻波, 对设备复杂度及精准度均要求较高。2012 年, Lei 等^[28]提供了一种允许在纳米光纤中使用波长为 980 nm 的两个反向传播激光束进行双向光学传输和纳米颗粒的可控定位的技术。借助于纤维表面的倏逝波, 悬浮在水中的颗粒通过梯度力被捕获到纤维上, 然后通过散射力沿纤维传输。同年, Li 等^[28]报道了沿着包括完整环结构的任意弯曲纳米纤维(直径 600 nm)的约 700 nm 直径聚苯乙烯球的光学递送。2019 年, Liu 等^[29]提出了一种由天然生物细胞组装而成的长度可调的生物输送带。利用倏逝波稳定地将纳米颗粒和细胞捕获在生物传送带表面, 并通过调整激光光源的功率, 使粒子或细胞可以沿着生物传送带双向传输。2020 年, Che 等^[30]使用椭圆聚焦激光束倾斜照射在衬底上的简单且具有成本效益的方案, 实现了用于微粒靶向递送的方向可控和距离可控的光传送器。2021 年, 申泽等^[31]设计一种具有鸟喙形的环形芯光纤光镊结构, 利用其弯曲结构增强了光纤侧边的倏逝场强度, 使其不仅可以

收稿日期: 2022-09-27; 修回日期: 2022-11-07; 录用日期: 2022-11-11; 网络首发日期: 2022-11-21

基金项目: 黑龙江省自然科学基金联合指导项目(LH2021F008)

通信作者: *jiangchunlei_nepu@163.com

在尖端捕获粒子,还可以在侧边捕获和运输粒子。2021年,Shan等^[32]完成了由空间光调制(SLM)或激光光纤耦合中的倾斜入射产生的由单个光纤形成的2~6个光阱的单细胞操作的动态建模和优化,以实现单个细胞的俘获传输和受控旋转;实验验证了LP₂₁模式的较大捕获力及优化的光束尺寸,为在单细胞水平上使用高阶光纤模式的最佳光学操纵提供了新的理解。以上方法大多在光纤上运输微粒,而同时具备定向发射功能的光镊少有涉及。利用双光纤探针的方法需要极其精密的操作以防光纤弯曲,组装较长传送带时需耗费时间用于捕获细胞;有些方法则不允许存在较大的弯曲损耗,对功率要求较高,避免纳米球在输送过程中逃逸;还有一些方法的光纤弯曲度及纳米光纤所需火焰条件等使得光纤端口制作难度较高,且需要考虑可重复性等问题。

本文提出一种具备发射功能的光学传送带,利用高阶LP₂₁模场将光场能量集中于光纤端口四周边缘,并通过拉制特殊的鳍豚形尖端构造长度可调控的输送结构,在低功率下进行聚苯乙烯微粒输送。此外,通过采用有限元分析法建立仿真模型来对比分析鳍豚形光纤和普通锥形光纤的光场分布,并结合麦克斯韦应力张量法推导光阱力公式,分析微粒的受力情况。通过仿真及实验验证了鳍豚形光纤的运输性能优于普通锥形光纤。

2 原理

2.1 LP₂₁模式激发原理

当传输波长大于截止波长时,单模光纤中只存在

基模LP₀₁;当传输波长小于截止波长时,单模光纤中也会相应地激发其他低阶或高阶模式光束。光纤中传播的模式数取决于传输光波在光纤中的归一化频率参数V:当V<2.405时,光纤中只有LP₀₁模式光束能够传播,其他模式均被截止;当2.405≤V≤3.832时,高阶LP₁₁模式光束将产生并传播;而当V>3.832时,LP₂₁模式出现。归一化频率参数V的计算公式为

$$V = \frac{2\pi\alpha}{\lambda} \sqrt{n_1^2 - n_2^2}, \quad (1)$$

式中: α 为单模光纤的纤芯半径; n_1 为纤芯折射率; n_2 为包层折射率。由式(1)可知,当激光波长λ=650 nm、单模光纤的纤芯半径α为4.5 μm、纤芯折射率n₁=1.467和包层折射率n₂=1.459时,V≈6.655>3.832,即单模光纤中存在高阶LP₂₁模式。图1(a)和(b)是使用波长为650 nm的激光分别在1550 nm和650 nm波长光纤中传输的LP₂₁模式和LP₀₁模式的光场轮廓分布图。从图1中可以看出:LP₂₁模式的光场能量并非和基模LP₀₁一样集中于中心轴上,其出射方向偏于中心轴向四周对称延伸,形成具有独特的四瓣强度呈中心对称分布的光场。高阶四瓣LP₂₁模式光束在光纤中具有高传输稳定性的强度分布,传输光纤的弯曲及扭转几乎不会导致此模式光强分布发生形变。此外,四光束光阱中轴向光阱的刚度较其他模式更强,在保证轴向捕获稳定性的同时,提高了横向捕获的稳定性。因此本文采用LP₂₁模式光束来对微粒进行捕获与运输。

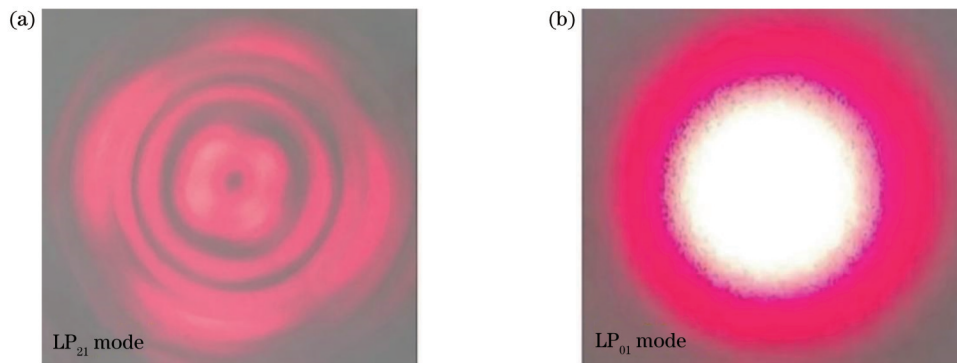


图1 两种模式光束的光场轮廓分布图。(a) LP₂₁模式光束;(b) LP₀₁模式光束;

Fig. 1 Light field profiles of two modes of light beams. (a) LP₂₁ mode beam; (b) LP₀₁ mode beam

2.2 鳍豚形光纤的制作

本文使用的鳍豚形光纤探针采用火焰加热技术由商用单模光纤G.652D拉制而成。首先,用纤维剥离器去除表面的光纤缓冲层和聚合物护套,得到长度为4 cm的裸纤维。然后采用不锈钢毛细管(内径约为0.9 mm,壁厚约为0.1 mm,长度约为120 mm)包裹裸纤维,以防止光纤断裂或弯曲翘起影响后续捕获操纵时的稳定性。将裸纤维放置于酒精灯火焰上加热约5 s,使其达到熔点,然后沿光轴以约为2.5 mm/s的速度

向两侧缓慢拉伸光纤,当光纤直径由125 μm变细至10 μm以内时,加快拉伸速度至约15 mm/s直至断裂,熔化纤维的表面张力在末端形成了鳍豚形尖端,其端口形状和具体参数如图2(a)所示。该鳍豚形光纤探针具有平滑的流动弧线形状并向前延伸出尖端,从而将发散的激光会聚在光纤两侧,其不仅可以增大出射光场的梯度,而且可以显著增强锥形侧面的倏逝场,提供较大的侧向捕获力,实现粒子的侧边定向运输。此外,本文制作了普通锥形光纤用于对比实验,且利用玻

璃毛细管使用同样的方法拉制了管道作为微粒运输的目标位置。普通锥形光纤及管道尺寸结构图如

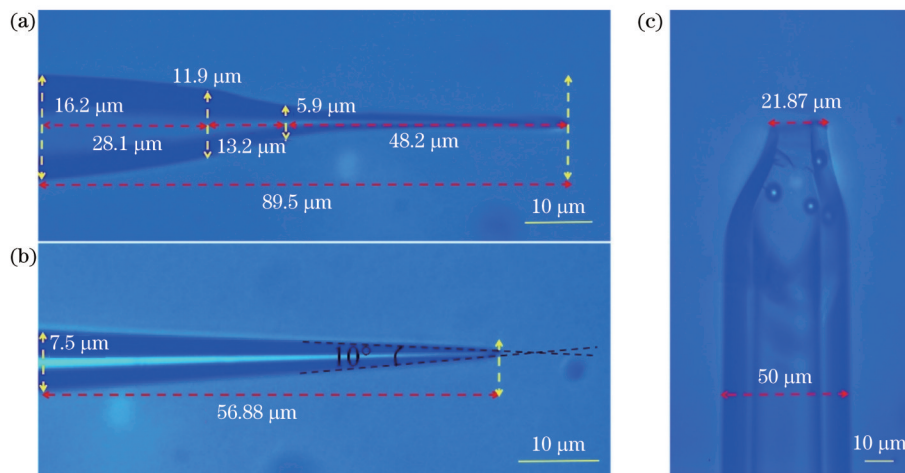


图2 所用光纤及管道尺寸图。(a)鳍豚形光纤探针图;(b)普通锥形光纤探针图;(c)目标输送管道尺寸图

Fig. 2 Size diagrams of optical fiber and pipe used. (a) Fin dolphin-shaped fiber probe pattern; (b) common tapered fiber probe; (c) dimension of target pipeline

为了验证鳍豚形光纤探针的优越性,本文使用有限元分析法对鳍豚形光纤探针和普通锥形光纤探针的矢量光场分布进行了仿真分析。其中仿真区域为 $120 \mu\text{m} \times 30 \mu\text{m}$ 的矩形区域,模型使用自由三角形网

格。光束在光纤中的传播方向是从左往右。光源的波长为650 nm,其端口输入功率为0.05 W/m;水、光纤探针、5 μm聚苯乙烯微粒的折射率分别设置为1.33、1.46和1.59。矢量光场分布仿真结果如图3(a)和(b)

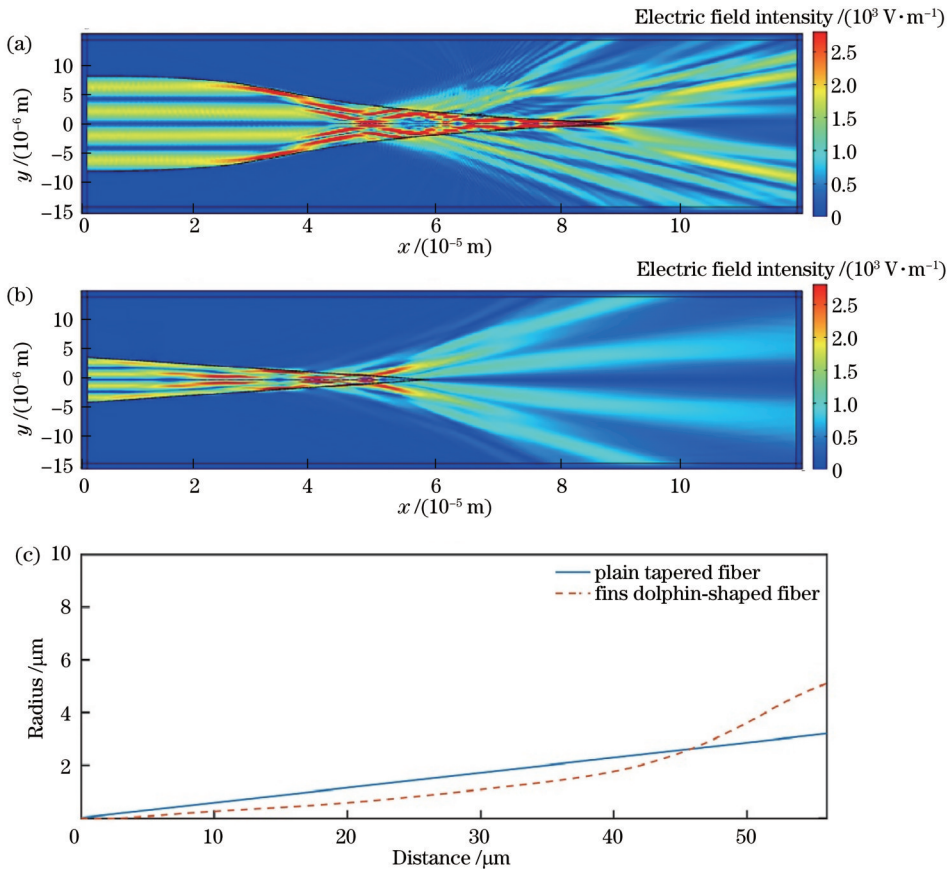


图3 光场仿真及直径对比图。(a)鳍豚形光纤光场分布图;(b)普通锥形光纤光场分布图;(c)光纤直径随距离的变化图

Fig. 3 Simulated light field and diameter comparison. (a) Light field distribution of fin dolphin-shaped fiber; (b) optical field distribution of common tapered fiber; (c) fiber diameter varying with distance

所示,图3(c)为鳍豚形光纤和普通锥形光纤的直径随端口距离的变化对比图。由光场仿真及直径对比图可清晰看出,鳍豚形光纤在直径为35~55 μm内存在较明显的变化,且直径突变处倏逝场明显增强,从弧形延伸至尖端顶部均存在较强侧向捕获力。对比普通锥形光纤可知,直径随距离呈较均匀的变化,靠近尖端处的倏逝场最强,随着尖端距离的增加,直径逐渐增大,光场逐渐减弱,且靠近顶部位置的聚焦区域向两侧偏移。因此,微粒运输过程中,前期倏逝场太弱致使光阱力较

小,微粒不易被捕获或者容易逃逸,后期靠近顶部时微粒易偏离航线并远离尖端,为后续粒子定向发射带来困难。不难推测,随着尖端锥角的增大,传送带作用距离会明显缩短。

此外,由于实验中使用650 nm红色激光光源,光纤断裂处散射红光会遮挡视线,如图4(a)所示。为避免红光影响观察,在采集数据过程中于CCD下方添加窄带滤光片,因此整体画面呈现淡蓝色,其效果如图4(b)所示。

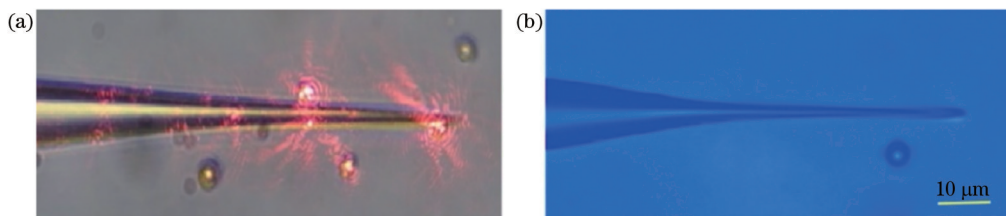


图4 加或者不加滤光片的实验对比图。(a)未加滤光片实验图;(b)加滤光片实验图

Fig. 4 Experimental figures without and with filter. (a) Experimental figure without filter; (b) experiment figure with filter

2.3 捕获力分析方法

微粒的捕获力主要是由于光场梯度分布引起的光梯度力和由于光的辐射压引起的光散射力。梯度力来自介质小球中的电偶极矩在不均匀电磁场中受到的力,它指向光场强度的最大处,使微粒朝向光功率密度最大的位置运动。散射力源于光在散射过程中与光子进行动量交换,微粒使光子动量发生改变,反之微粒自身受到该动量改变的反作用力。散射力的方向沿着光的传播方向,从而使微粒沿着光束的传播方向运动。梯度力和散射力的合力被称为捕获力。捕获力与光的波长、粒子属性及粒子尺寸等因素密切相关。本研究使用有限元分析法,通过解麦克斯韦方程对光纤矢量光场分布和变化进行精确描述,再通过麦克斯韦应力张量法分析粒子的受力情况。根据麦克斯韦方程,电场 E 的本征值方程由式(2)得到:

$$\nabla \cdot (\nabla \cdot E) - k_0^2 n^2 E = 0, \quad (2)$$

式中: k_0 为波数; n 为材料折射率。通过积分粒子表面的麦克斯韦应力张量,可计算出作用在物体上的光学力。而应力张量 $\langle T_M \rangle$ 为

$$\langle T_M \rangle = DE^* + HB^* - \frac{1}{2}(DE^* + HB^*)I, \quad (3)$$

式中: D 为电场位移; H 为磁场; B 表示磁通量; I 是各向同性张量; E^* 、 H^* 、 B^* 分别是 E 、 H 、 B 的复共轭。应用本构关系 $D = \epsilon_r \epsilon_0 E$ (ϵ_r 为相对介电常数, ϵ_0 为真空介电常数)和 $B = \mu_r \mu_0 H$ (μ_r 为相对磁导率, μ_0 为真空磁导率),式(3)可以改写为

$$T_k = \epsilon_r \epsilon_0 E_k E_k^* + \mu_r \mu_0 H_k H_k^* - \frac{1}{2}(\epsilon_r \epsilon_0 E_k E_k^* + \mu_r \mu_0 H_k H_k^*)\delta_k, \quad (4)$$

式中: $k=1, 2, 3$; E_k 和 H_k 为电场和磁场的第 k 个分量; δ_k 是克罗内克脉冲函数。对指标 k 求和,故作用在物

体上的光学力 F 定义为

$$F = \oint_S (\langle T_M \rangle \cdot \mathbf{n}_S) dS, \quad (5)$$

式中: \mathbf{n}_S 为指向物体表面 S 的法向量^[22]。通过高斯定理(或散度定理)可知,作用在体积为 V 的粒子的作用力可换算为作用在其闭合曲面 S 上的力。

3 实验

3.1 实验装置

实验装置如图5所示。本文采用工作波长为650 nm的激光作为光源,光源输出功率 P 可在0~90 mW以内调节。首先将650 nm波长的激光光源耦合到典型工作波长为1550 nm的G. 652D单模光纤(光纤直径:125 μm,纤芯直径:9 μm)一端,并对单模光纤的另一端进行火焰加热和拉伸,制作成鳍豚形端口光纤探针用于微粒的捕获运输。将鳍豚形光纤探针固定在精密的五维平台上,从而实现光纤探针的精确定位。同时用不锈钢铠甲包裹光纤探针,防止光纤探针断裂和弯曲。随后将光纤探针浸入悬浮液中,悬浮液是通过蒸馏水稀释直径为5 μm的聚苯乙烯微粒并加以超声处理制作而成。最后通过连接在计算机上的CCD摄像机来实时观察细胞的光学捕获,并记录实验图像。

3.2 实验结果及分析

本实验借助蓝丁胶在盖玻片与载玻片之间形成一个长约2 cm、高约1~2 mm的正方形腔室,以减弱粒子在溶液中的布朗运动、减小空气对溶液的蒸发力。实验过程如图6所示:当时间 t 在0~5 s内,直径为5 μm的聚苯乙烯微粒被稳定捕获在距离光纤尖端约40 μm的侧边位置,此时光纤尖端的输出功率约在10 mW以内;当 $t=5$ s时,微粒开始向前运动;当 $t=25$ s时,微粒运动

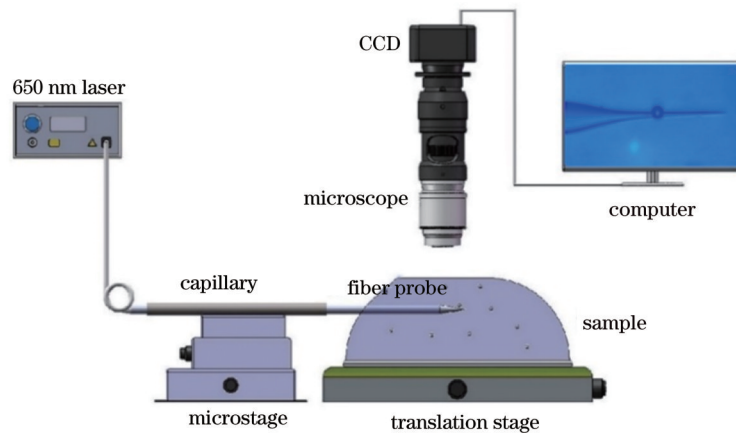


图5 实验装置图。

Fig. 5 Diagram of experimental setup

至光纤尖端位置并向外推出,其平均运动速度为 $2.33 \mu\text{m}/\text{s}$ 。图6(a)~(e)显示微粒的运输过程,

图6(f)~(j)展示了微粒被定向输送到目标管道中的过程,其中虚线圆圈为参考点,帮助观察粒子的运输。

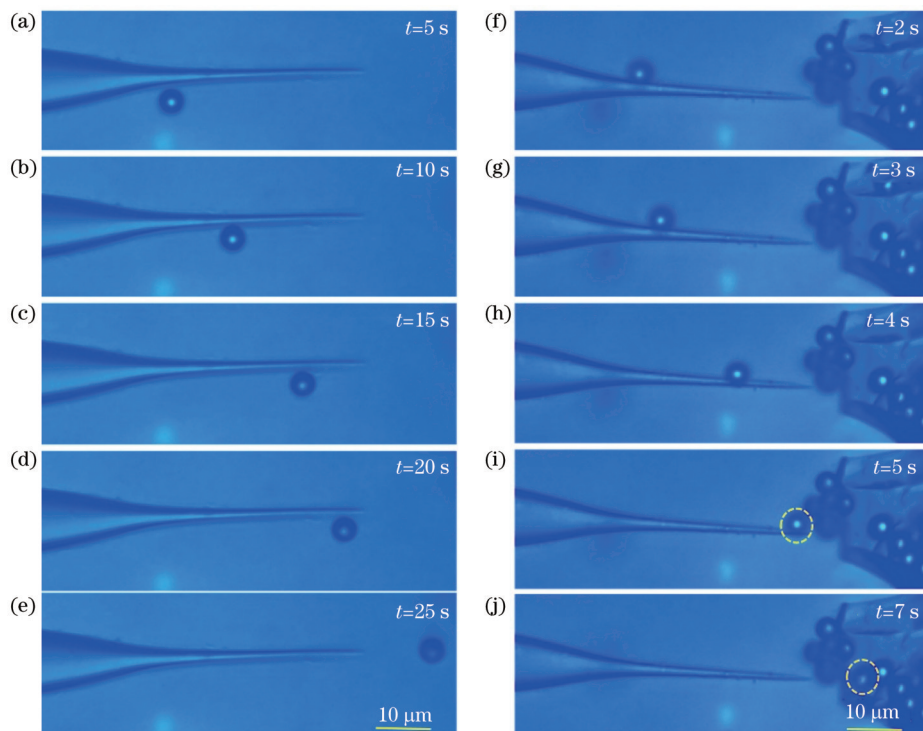


图6 微粒运输实验过程图。(a)~(e)微粒运输过程图;(f)~(j)微粒定向运输至管道图

Fig. 6 Process diagrams of particle transport experiment. (a)–(e) Diagrams of particle transport process; (f)–(j) directional transport of particles to pipe

为了体现鳍豚形光纤的运输特性,拉制了锥角约为 10° 的普通锥形光纤,在不同大小的输出功率下分别进行对比实验,如图7和图8所示。实验结果显示:当光纤端口的输出功率约为 6.5 mW ,鳍豚形光纤和普通锥形光纤的平均运输速度分别约为 $12.5 \mu\text{m}/\text{s}$ 和 $3.14 \mu\text{m}/\text{s}$;当光纤端口的输出功率约为 20 mW 时,鳍豚形光纤和普通锥形光纤的平均运输速度分别为 $22.5 \mu\text{m}/\text{s}$ 和 $12.75 \mu\text{m}/\text{s}$ 。为了清晰表示两种不同光纤的运输特性,制作了光纤端口输出功率与平均运输

速度的对比曲线,如图9所示。分析可知,鳍豚形光纤因其直径突变结构在弧形处的光场泄漏更多,因而在光纤端口输出功率相同的情况下,鳍豚形光纤运输特性均优于普通锥形光纤。

为了定量研究两种光纤探针侧边粒子的受力情况对微粒运输速度的影响,本文对两种不同光纤探针侧边捕获微粒的受力情况进行仿真分析,仿真结果如图10和图11所示。图10(a)与图11(a)分别为鳍豚形光纤和普通锥形光纤侧边粒子的受力情况,图10(b)与

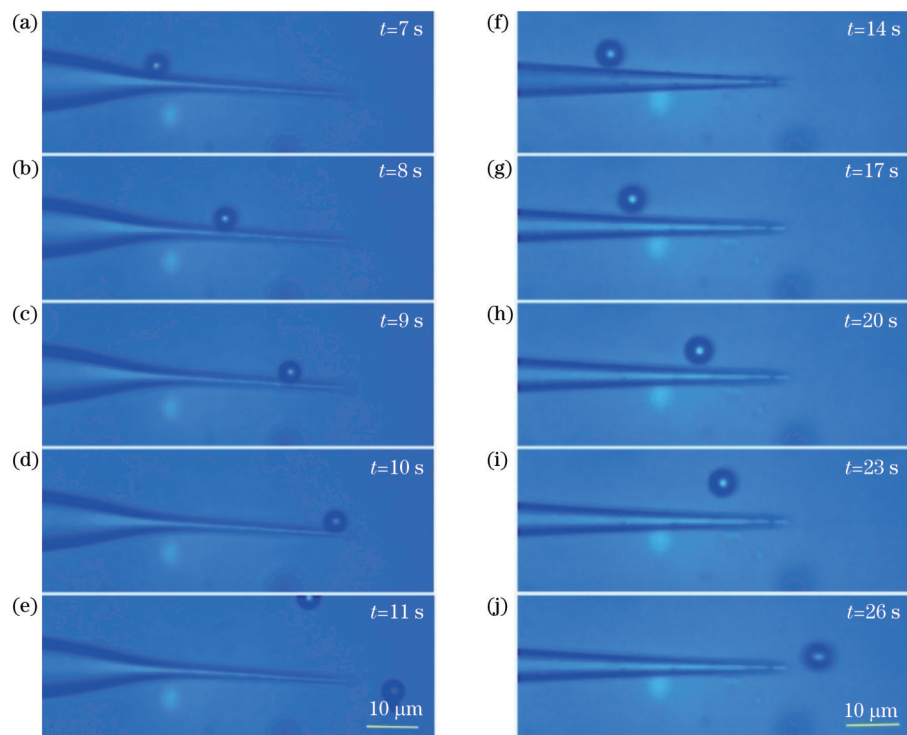


图 7 低功率下两种光纤运输对比图。(a)~(e) 鳍豚形光纤的运输过程图;(f)~(j) 普通锥形光纤的运输过程图

Fig. 7 Comparison of transport of two types of fiber at low power. (a)–(e) Diagrams of transport process of fin dolphin-shaped fiber; (f)–(j) diagrams of transport process of normal tapered fiber

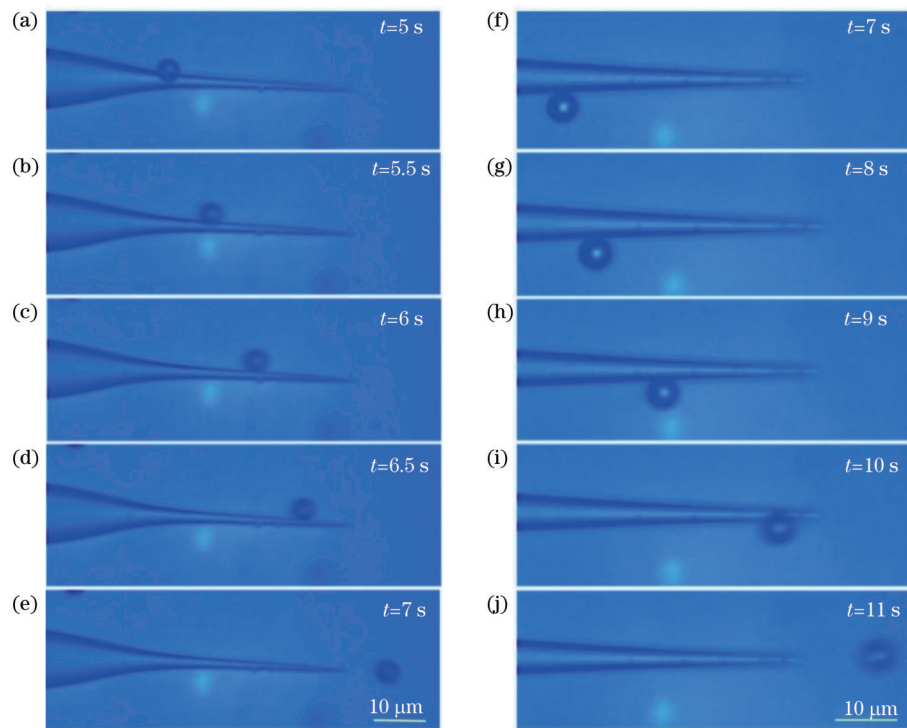


图 8 高功率下两种光纤运输对比图。(a)~(e) 鳍豚形光纤的运输过程图;(f)~(j) 普通锥形光纤的运输过程图

Fig. 8 Comparison of transport of two types of fiber at high power. (a)–(e) Diagrams of transport process of fin dolphin-shaped fiber; (f)–(j) diagrams of transport process of normal tapered fiber

图 11(b) 分别为鳍豚形光纤和普通锥形光纤尖端轴向受力。

由图 10(a)与图 11(a)可知,微粒在两种光纤侧边

受到一个逐渐变大的正方向力,即微粒沿光纤侧边被推向光纤端口,且鳍豚形光纤侧边对微粒产生的力大于普通锥形光纤,从而导致鳍豚形光纤侧边粒子的运

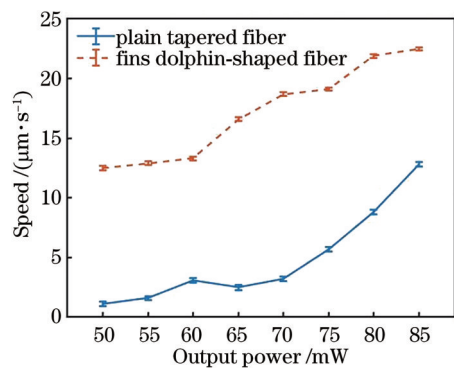


图9 平均运输速度随输出功率的变化曲线图

Fig. 9 Plot of average transport speed varying with output power

动速度大于普通锥形光纤侧边粒子的运动速度。微粒运动至光纤尖端后,受到一个逐渐变小的正方向力,即

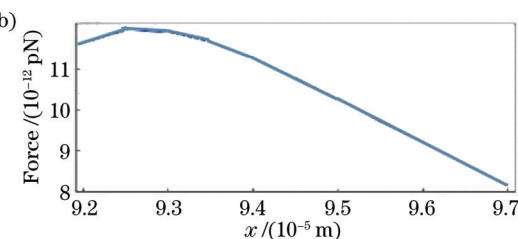
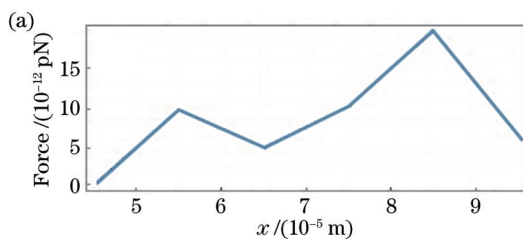


图10 鳍豚形光纤微粒受力图。(a)侧向受力曲线图;(b)轴向受力曲线图

Fig. 10 Force diagrams of fin dolphin-shaped fiber particles. (a) Lateral force curve; (b) axial force curve

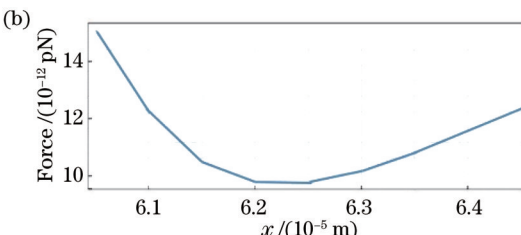
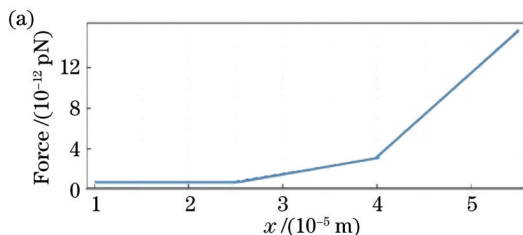


图11 普通锥形光纤微粒受力图。(a)侧向受力曲线图;(b)轴向受力曲线图

Fig. 11 Force diagrams of ordinary tapered fiber particle. (a) Lateral force curve; (b) axial force curve

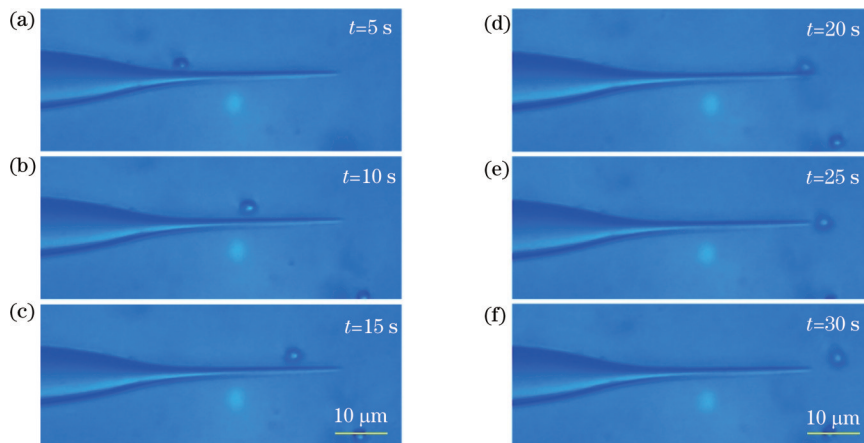


图12 光纤传送带输送小球藻细胞过程图

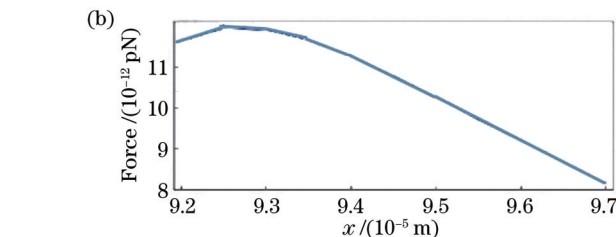
Fig. 12 Transport of *Chlorella* cells by fiber optic conveyor belt

微粒沿光纤尖端的轴向向外运动。

为了更好地与生物医学相结合,本文使用鳍豚形光纤输送了直径为3~5 μm的小球藻细胞。其中,光纤端口输出功率约为8.5 mW,运输过程如图12(a)~(f)所示,实验结果显示鳍豚形光纤在低功率下依然能稳定运输。细胞的定向输送为医学及大分子领域发展开拓了新的方向。

4 结 论

设计了一种鳍豚形光纤光镊结构,通过高阶LP₂₁模式光束增强光纤侧边边缘的光场强度以实现光纤传送带功能,最终微粒被运输至尖端处并被弹射出去。应用有限元法仿真光镊的光场强度分布,对比了不同形状条件下光镊的光场图。结果表明,光纤端口处弧形结构显著增强了光纤侧边的倏逝场强度。采用麦克斯韦应力张量法计算光镊对粒子的捕获力,并对比普

Fig. 12 Transport of *Chlorella* cells by fiber optic conveyor belt

通锥形光纤,分析了两种不同光纤的侧边捕获力对粒子运输速度的影响。结果证实该特殊结构光纤光镊可以在侧边捕获、运输粒子,并由尖端发射粒子。该研究为微粒运输和微粒发射功能的结合拓展了方向,同时为新型光纤光镊的研究及生物细胞学领域提供了新的可能。

参 考 文 献

- [1] Ashkin A, Dziedzic J M. Optical trapping and manipulation of viruses and bacteria[J]. *Science*, 1987, 235(4795): 1517-1520.
- [2] Bjorkholm J E, Freeman R R, Ashkin A, et al. Observation of focusing of neutral atoms by the dipole forces of resonance-radiation pressure[J]. *Physical Review Letters*, 1978, 41(20): 1361-1364.
- [3] Gauthier R C. Optical trapping: a tool to assist optical machining [J]. *Optics & Laser Technology*, 1997, 29(7): 389-399.
- [4] Crocker J C, Grier D G. When like charges attract: the effects of geometrical confinement on long-range colloidal interactions[J]. *Physical Review Letters*, 1996, 77(9): 1897-1900.
- [5] Wojdyla M, Raj S, Petrov D. Absorption spectroscopy of single red blood cells in the presence of mechanical deformations induced by optical traps[J]. *Journal of Biomedical Optics*, 2012, 17(9): 097006.
- [6] Landenberger B, Höfemann H, Wadle S, et al. Microfluidic sorting of arbitrary cells with dynamic optical tweezers[J]. *Lab on a Chip*, 2012, 12(17): 3177-3183.
- [7] 张聿全, 张硕硕, 阎长俊, 等. 飞秒光镊技术研究与应用进展 [J]. 中国激光, 2021, 48(19): 1918001.
Zhang Y Q, Zhang S S, Min C J, et al. Research progress of femtosecond optical tweezers and their applications[J]. *Chinese Journal of Lasers*, 2021, 48(19): 1918001.
- [8] 韩翔, 陈鑫麟, 熊威, 等. 真空光镊系统及其在精密测量中的研究进展[J]. 中国激光, 2021, 48(4): 0401011.
Han X, Chen X L, Xiong W, et al. Vacuum optical tweezers system and its research progress in precision measurement[J]. *Chinese Journal of Lasers*, 2021, 48(4): 0401011.
- [9] Xia Y Q, Tang Y, Yu X, et al. Label-free virus capture and release by a microfluidic device integrated with porous silicon nanowire forest[J]. *Small*, 2017, 13(6): 1603135.
- [10] Zhao X T, Shi Y, Pan T, et al. *In situ* single-cell surgery and intracellular organelle manipulation via thermoplasmonics combined optical trapping[J]. *Nano Letters*, 2022, 22(1): 402-410.
- [11] Pan T, Lu D Y, Xin H B, et al. Biophotonic probes for bio-detection and imaging[J]. *Light: Science & Applications*, 2021, 10: 124.
- [12] Yuan Y F, Wu G, Li X, et al. Effects of twisting and bending on LP₂₁ mode propagation in optical fiber[J]. *Optics Letters*, 2011, 36(21): 4248-4250.
- [13] Taylor R S, Hnatovsky C. Particle trapping in 3-D using a single fiber probe with an annular light distribution[J]. *Optics Express*, 2003, 11(21): 2775-2782.
- [14] Reddy I V A K, Bertoncini A, Liberale C. 3D micro-printed ultra-compact single-fiber Optical tweezers[C]//Biophotonics Congress 2021, April 12-16, 2021, Washington, DC. Washington, DC: Optica Publishing Group, 2021: AM1D.6.
- [15] Valdez L, Shum H, Ortiz-Rivera I, et al. Solutal and thermal buoyancy effects in self-powered phosphatase micropumps[J]. *Soft Matter*, 2017, 13(15): 2800-2807.
- [16] Wilhelm S, Tavares A J, Dai Q, et al. Analysis of nanoparticle delivery to tumours[J]. *Nature Reviews Materials*, 2016, 1: 16014.
- [17] Duan W T, Wang W, Das S, et al. Synthetic nano- and micromachines in analytical chemistry: sensing, migration, capture, delivery, and separation[J]. *Annual Review of Analytical Chemistry*, 2015, 8: 311-333.
- [18] Liu X S, Huang J B, Li Y C, et al. Rotation and deformation of human red blood cells with light from tapered fiber probes[J]. *Nanophotonics*, 2016, 6(1): 309-316.
- [19] Lee C Y, Yen C T, Chu K W, et al. A novel 4H-SiC Trench MOS Barrier Schottky rectifier fabricated by a two-mask process [C]//2013 25th International Symposium on Power Semiconductor Devices & IC's (ISPSD), May 26-30, 2013, Kanazawa, Japan. New York: IEEE Press, 2013: 171-174.
- [20] Mandal S, Serey X, Erickson D. Nanomanipulation using silicon photonic crystal resonators[J]. *Nano Letters*, 2010, 10 (1): 99-104.
- [21] Yang A H J, Moore S D, Schmidt B S, et al. Optical manipulation of nanoparticles and biomolecules in sub-wavelength slot waveguides[J]. *Nature*, 2009, 457(7225): 71-75.
- [22] Frawley M C, Gusachenko I, Truong V G, et al. Selective particle trapping and optical binding in the evanescent field of an optical nanofiber[J]. *Optics Express*, 2014, 22(13): 16322-16334.
- [23] Lei H X, Xu C, Zhang Y, et al. Bidirectional optical transportation and controllable positioning of nanoparticles using an optical nanofiber[J]. *Nanoscale*, 2012, 4(21): 6707-6709.
- [24] Baaske M D, Foreman M R, Vollmer F. Single-molecule nucleic acid interactions monitored on a label-free microcavity biosensor platform[J]. *Nature Nanotechnology*, 2014, 9(11): 933-939.
- [25] Wang G H, Ying Z F, Ho H P, et al. Nano-optical conveyor belt with waveguide-coupled excitation[J]. *Optics Letters*, 2016, 41(3): 528-531.
- [26] Ruffner D B, Grier D G. Optical conveyors: a class of active tractor beams[J]. *Physical Review Letters*, 2012, 109(16): 163903.
- [27] Čížmár T, Garcés-Chávez V, Dholakia K, et al. Optical conveyor belt for delivery of submicron objects[J]. *Applied Physics Letters*, 2005, 86(17): 174101.
- [28] Li Y, Xu L L, Li B J. Optical delivery of nanospheres using arbitrary bending nanofibers[J]. *Journal of Nanoparticle Research*, 2012, 14(4): 799.
- [29] Liu X S, Wu Y, Xu X H, et al. Bidirectional transport of nanoparticles and cells with a bio-conveyor belt[J]. *Small*, 2019, 15(50): 358-362.
- [30] Che Z, Zhu W G, Huang Y M, et al. Distance-controllable and direction-steerable opto-conveyor for targeting delivery[J]. *Photonics Research*, 2020, 8(7): 1124-1133.
- [31] 申泽, 成煜, 邓洪昌, 等. 鸟喙形环形芯光纤光镊粒子捕获受力分析[J]. 光学学报, 2021, 41(18): 1808001.
Shen Z, Cheng Y, Deng H C, et al. Analysis of trapping force of beak-shaped optical tweezers with annular core fibers for particles[J]. *Acta Optica Sinica*, 2021, 41(18): 1808001.
- [32] Shan Z H, Yao S N, Zhang E F, et al. High-order fiber mode beam parameter optimization for transport and rotation of single cells[J]. *Micromachines*, 2021, 12(2): 226.

Fin Dolphin-Shaped Transmitting Fiber Conveyor Belt Based on High-Order LP₂₁ Mode

Gao Bingkun, Rong Yufei, Jiang Chunlei*, Chen Peng, Shui Huasheng, Wu Hao,
Dong Taiji, Sun Yu, Yan Wendi

College of Electrical Information Engineering, Northeast Petroleum University, Daqing 163318, Heilongjiang,
China

Abstract

Objective Optical tweezers were first proposed by Arthur Ashkin in 1986 and were first used in the biological science field in the late 1980s. Since then, optical tweezers have been applied to atomic physics, micromachining, chemistry, biomedicine, and microelectromechanical systems. Meanwhile, on the basis of application development, other new optical tweezer systems such as femtosecond and vacuum laser systems have also been derived. In addition, they have been widely combined with new biomedical technologies in recent years and used for pathological detection of cells, single-cell microsurgery, and designs of biological lasers, cell-based biological photonic waveguides, and biological micro-lenses by using biological entities such as viruses, cells, and tissues. With the rapid development of the microoperation field, functional requirements of fiber optic tweezers are becoming higher and higher, so it is particularly important to improve their utilization efficiency and integration. A variety of methods have been proposed to transport particles, and some of which are made by using double optical fibers to capture cell chains and make a conveyor belt. Some pull the bending port to enhance the evanescent field, while others pull micro-nano fibers and control the power of two lasers to transport them. Most of them transport particles over optical fibers, but optical tweezers with directional emission functions are less involved. Moreover, the use of dual fiber probes requires an extremely precise operation to prevent bending, and it takes time to capture cells when assembling long conveyor belts. Or the bending degree and flame conditions required by nanofibers make it difficult to fabricate fiber ports and thus need to consider repeatability and other issues. To solve the above problems, this paper designs a fin dolphin-shaped fiber optical tweezer structure, which combines with a high-order LP₂₁ mode to realize the function of a fiber conveyor belt. This method is simple and provides a new possibility for optical fiber manipulation.

Methods In this paper, a light source of 650 nm is fed into a high energy ratio LP₂₁ mode in a G. 652D fiber with a typical operating wavelength of 1550 nm. The characteristic of the LP₂₁ mode light field is that the outgoing direction is biased towards the central axis and extends symmetrically around, which forms a light field with a unique four-petal center symmetric intensity distribution. Moreover, the high-order four-petal LP₂₁ mode beam has the intensity distribution of high transmission stability in the fiber, and the bending and torsion of the transmission fiber can hardly cause the deformation of the intensity distribution of this mode. In addition, the stiffness of the axial optical trap in the four-beam optical trap is stronger than that in other modes, which not only ensures the stability of the axial capture but also improves the stability of the transverse capture. Therefore, the LP₂₁ mode beam is used in this paper to capture and transport particles. In addition, in order to ensure the stability of particle transport, a fin dolphin-shaped fiber probe is designed, which has a smooth flow arc shape and extends the tip forward, so as to converge the diverging laser on both sides of the fiber. At the same time, this paper makes an ordinary conical fiber for comparative experiments to study the transportation performance of the fin dolphin-shaped fiber and measures the transportation speed of the two kinds of fiber under high and low power. A glass capillary tube is used as the target location for particle transport. The feasibility of the experiments is analyzed by the finite element method.

Results and Discussions The experimental and simulation results show that the evanescent field at the sudden change of the diameter of the fin dolphin-shaped fiber is significantly enhanced, and it extends from the arc to the top of the tip, with a strong lateral capture force. Compared with common tapered fibers, the evanescent field near the tip is the strongest. With the increase in the tip distance, the diameter gradually increases, and the light field gradually weakens. Furthermore, the focusing region near the top is shifted to both sides. Therefore, in the particle transportation process, the evanescent field is too weak in the early period, which results in a small light trapping force, and particles are not easy to be captured or escape. In the late period, when particles are near the top, it is easy to deviate from the course and be away from the tip, which brings difficulties for the directional emission of subsequent particles. Several comparative experiments are carried out under different optical power. The results show that the fin dolphin-shaped fiber has more advantages in

transportation speed and stability.

Conclusions In this paper, we design a fin dolphin-shaped fiber optical tweezer structure and enhance the optical field intensity of the side edge of the fiber through a high-order LP₂₁ mode beam to achieve the function of a fiber conveyor belt, and particles are finally transported to the tip for ejection. The finite element method is used to simulate the intensity distribution of the optical field, which shows that the arc structure at the fiber port has significantly enhanced the evanescent field intensity at the side of the fiber. The influence of the side trapping force on the particle transport speed is analyzed by comparing it with conventional conical fiber. The results show that the special structure of the fiber is superior. It expands the direction of the combination of particle transport and particle emission and provides a new possibility for the research on new fiber optic tweezers and the biological cytology field.

Key words fiber optics; particle transport; directional control; fin dolphin-shaped fiber; LP₂₁ mode